

# Structural and Magnetic Studies of Mg<sup>+2</sup> doped NiFe<sub>2</sub>O<sub>4</sub> using Citrate Precursor Method

Mohd Khizar Syed<sup>1</sup>, S. Abdul Khader<sup>2\*</sup>, Chishty Syed Qadeeruddin<sup>3\*</sup>

<sup>1</sup>Department of Physics, Kohinoor College, Khuldabad, Aurangabad-431101, Maharashtra, India.

<sup>2</sup>Department of P.G Studies and Research in Physics, MSCWM, Mysore-570005, Karnataka. India.

<sup>3</sup>Department of Physics, Dr Rafiq Zakaria College for Women, Aurangabad, Maharashtra, India.

\*Corresponding Author (s)

## Abstract.

Mg<sup>+2</sup> doped NiFe<sub>2</sub>O<sub>4</sub> ferrite nano-particles with the basic composition Mg<sub>x</sub>Ni<sub>1-x</sub>Fe<sub>2</sub>O<sub>4</sub> (x=0, 0.25, 0.5, 0.75, 1) were synthesized using nitrate-citrate method, which is also known as auto-combustion method. Synthesized samples, sintered at 900°C were investigated for various properties through its structural, dielectric and magnetic studies. Phase of the synthesized samples were probed by X-ray diffraction (XRD) studies. Peaks observed in the PXRD spectrum confirms the single phase spinel cubic structure for the pure and Mg<sup>+2</sup> doped NiFe<sub>2</sub>O<sub>4</sub> samples. Using FESEM, surface morphology of the samples has been investigated. Using Hioki make LCR Hi-Tester 3250, various dielectric parameters such as dielectric permittivity ( $\epsilon'$ ), dielectric loss tangent ( $\tan \delta$ ) were investigated as a function of frequency and Mg<sup>+2</sup> concentration at room temperature, over the frequency range 100 Hz to 1 MHz. Frequency dependence of  $\epsilon'$  and  $\tan \delta$  is in accordance with the Maxwell-Wagner type interfacial polarization. Electrical conductivity ( $\sigma_{ac}$ ) is deduced from the measured dielectric data, and found that the conduction mechanism in Mg<sub>x</sub>Ni<sub>1-x</sub>Fe<sub>2</sub>O<sub>4</sub> nanoferrites are in conformity with the electron hopping model. Using vibrating sample magnetometer (VSM), for the proposed ferrites, magnetic properties were investigated.

**Keywords:** Combustion; Ferrites; Magnetic properties; Hopping Model.

## 1. INTRODUCTION

Nano-crystalline spinel ferrites are the magnetic oxides with excellent electrical and magnetic properties, can be easily tuned by controlling the size of synthesized particles using various preparation techniques. Because of their imperative technological and bio-medical applications they are employed in numerous devices like radiofrequency circuits, ferro-fluids, hyperthermia, cores of transformer, microwave antennas, magnetic recording [1-4].

Ferri-magnetic materials, mainly consisting of ferric oxide (Fe<sub>2</sub>O<sub>3</sub>) are known as ferrites and have spinel cubic structure. Ferrites exhibit magnetic hysteresis (M-H curve) and also exhibit spontaneous magnetization. Electrical and magnetic properties of spinel ferrites is because of distribution of cations among the available crystallographic lattice sites such as tetrahedral (A) and octahedral (B) sites [5]. For any ferrites, its properties depends upon the various parameters such as preparation technique adopted, type of organic fuel used, sintering temperature and sintering time, the type of environment such as in air, or inert gas in which the samples were synthesized, etc.

Nickel ferrite belongs to inverse spinel with Ni<sup>+2</sup> at octahedral (B-site) and Fe<sup>+3</sup> ions distributed equally in both, tetrahedral (A-site) and octahedral sites (B-site) [6]. Nickel and Magnesium ferrites are used in numerous electronic device applications because of their high permeability, high electrical resistivity, mechanical hardness, and chemical stability [7].

Magnesium ferrite is among the technologically important ferrites with spinel cubic structure, which is used in number of application oriented devices such as in field sensors, heterogeneous catalysis, and in gas sensors [8-10].

In our present study, samples with the basic composition Mg<sub>x</sub>Ni<sub>1-x</sub>Fe<sub>2</sub>O<sub>4</sub> (x=0, 0.25, 0.5, 0.75, 1) were prepared using nitrate-citrate auto-combustion method, which involves exothermic and self-propagating thermally-induced reaction of a xerogel, obtained from aqueous solutions containing metallic nitrates which acts as oxidizer and an organic fuel. Stoichiometric proportions between fuel and metallic nitrates are calculated according to the valencies of the reacting elements so as to provide the relation of oxidizer/fuel equal to one [11-12]. Here, metallic nitrates are preferred as starting materials which are also known as precursors, because of their water-soluble nature, have low ignition temperatures and are easy to prepare.

## 2. MATERIALS AND METHODS

Mg<sub>x</sub>Ni<sub>1-x</sub>Fe<sub>2</sub>O<sub>4</sub> nano ferrite (where x=0.0, 0.25, 0.5, 0.75, 1.0) powders were prepared using auto-combustion method. Precursors for starting the materials synthesis are Nickel Nitrate (Ni(NO<sub>3</sub>)<sub>2</sub>·6H<sub>2</sub>O), Ferric Nitrate (Fe(NO<sub>3</sub>)<sub>2</sub>·9H<sub>2</sub>O), Magnesium Nitrate (Mg(NO<sub>3</sub>)<sub>2</sub>·6H<sub>2</sub>O), Citric acid (C<sub>6</sub>H<sub>8</sub>O<sub>7</sub>·H<sub>2</sub>O), all chemicals are of AR Grade with purity more than 99%.

Aqueous solutions of metallic nitrates and Citric acid, which is here taken as organic fuel needed for auto-combustion reaction and are taken as per the stoichiometry. Equi-molar citric acid was added into the aqueous solution of metallic nitrates. Aqueous solution containing redox mixture was taken in a silica crucible and is allowed in to a muffle furnace, which was already pre-heated to a temperature of 550°C. Redox mixture finally yields porous and fluffy voluminous ferrite powder. Obtained fluffy material was ground to get ferrite powders. As-burnt ash was sintered at 900°C for 4 hours to get better crystallization and homogeneous cation distribution in the proposed spinel and finally ground to get Mg<sup>+2</sup> doped nano powders of NiFe<sub>2</sub>O<sub>4</sub>.

Phase of the pure and Mg<sup>+2</sup> doped NiFe<sub>2</sub>O<sub>4</sub> samples were investigated by X-ray diffraction (XRD) studies using Bruker AXS D8 Advance X-ray diffractometer (using Cu-K<sub>α</sub> radiation, λ=1.5406 Å), a working voltage of 40kV at 40mA of current. Diffraction data were collected in the 2θ range 10-70°. Morphology of the sintered samples has been investigated using Field Emission Scanning Electron Microscope (JEOL JSM 6700). Parallel capacitance, C<sub>p</sub> and dissipation factor, tanδ as a function of frequency in the range 100 Hz-1 MHz were measured using a precision LCR meter. Real and imaginary parts of dielectric permittivity (ε') and (ε'') were computed using the formulae [13]

$$\epsilon' = Ct/\epsilon_0 A \quad (1)$$

$$\epsilon'' = \epsilon' \tan \delta \quad (2)$$

Where, t is the thickness and A the area of the pellet.

The ac conductivity, σ<sub>ac</sub> was determined from the dielectric loss factor using a relation

$$\sigma_{ac} = \omega \epsilon_0 \epsilon'' \quad (3)$$

Where, ε<sub>0</sub> is the vacuum permittivity and ω = 2πf with f being frequency.

### 3. RESULTS AND DISCUSSION

#### 3.1 Phase and Surface Morphology

Presence of (220), (311), (400), (422), (511), (440) and (533) planes in the diffraction patterns confirms the spinel cubic structure for all the sintered samples. Obtained PXRD patterns of Mg<sub>x</sub>Ni<sub>1-x</sub>Fe<sub>2</sub>O<sub>4</sub> (where x=0.0, 0.25, 0.5, 0.75, 1.0) ferrite series are presented in Figure 1. Presence of (220), (311), (400), (422), (511), (440) and (533) planes indexed for the cubic phase of spinel ferrites [ICSD: 109303 for NiMgFe<sub>2</sub>O<sub>4</sub>, ICSD: 240838 for MgFe<sub>2</sub>O<sub>4</sub> and Ref Code No: 01-076-9748 for NiFe<sub>2</sub>O<sub>4</sub>]. From the X-ray diffractogram and obtained diffraction data, mean crystallite size was calculated from the most intense peak (311) using the Scherrer's formula, D=kλ/βcosθ; where 'D' is the mean crystallite size, β is the full width at half maximum (FWHM) of the peak (311) and k=0.9 is the instrumental constant [14]. Calculated average crystallite size for all the samples is of the order of 30 nm. From inter-planar spacing (d) and miller indices (hkl) values [15-16], the lattice parameters were computed using, lattice constant, a= d<sub>hkl</sub>(h<sup>2</sup>+k<sup>2</sup>+l<sup>2</sup>)<sup>1/2</sup>. XRD density (ρ<sub>XRD</sub>) was calculated for each sample using the relation ρ<sub>XRD</sub>=8M<sub>w</sub>/(N<sub>A</sub>a<sup>3</sup>), here 8 represents the number of chemical formulas per unit cell, M<sub>w</sub> is the molecular weight of each ferrite sample, N<sub>A</sub> is Avogadro's number and 'a<sup>3</sup>' is the unit cell volume [17] and are shown in Table 1. Doping with smaller Ni<sup>+2</sup> ions (ionic radii is 0.69Å) with larger Mg<sup>+2</sup> ions (ionic radii of Mg<sup>+2</sup> is 0.72Å) causes a slight variation in lattice constant and mean crystallite size, it is observed that both mean crystallite size and lattice constant decreases with the increase in the concentration of Mg<sup>+2</sup> ions.

Hopping length between the metal ions at the tetrahedral A-site (L<sub>A</sub>) and octahedral B-site (L<sub>B</sub>) can be calculated using the relation [18]:

$$L_A = a_{exp} \sqrt{3}/4 \quad \text{and} \quad L_B = a_{exp} \sqrt{2}/4 \quad (4)$$

Values of hopping lengths are tabulated in Table 1(a), the variation of hopping length changes with the Mg<sup>+2</sup> concentration, similar behavior as that of lattice constant is observed. In case of spinel structure, the oxygen positional parameter (u) has a value in the neighborhood of 0.375Å for which the arrangement of O<sup>-2</sup> ions are equal exactly a cubic closed packing. Using the experimental values of lattice constant 'a' and oxygen positional parameter 'u', the tetrahedral and octahedral bond lengths (d<sub>AO</sub> and d<sub>BO</sub>), tetrahedral edge (d<sub>AE</sub>), shared octahedral edge (d<sub>BE</sub>) and unshared octahedral edge (d<sub>BEU</sub>) are computed using the below mentioned relations and are recorded in Table 1(b).

$$d_{AO} = a\sqrt{3}(u-0.25) \quad ; \quad d_{BO} = a\left(3u^2 - \frac{11u}{4} + \frac{43}{64}\right)^{0.5} \quad (5a)$$

$$d_{AE} = a\sqrt{2}(2u-0.5) \quad ; \quad d_{BE} = a\sqrt{2}(1-2u) \quad (5b)$$

$$d_{BEU} = a(4u^2 - 3u + 11/16)^{0.5} \quad (5c)$$

Microstructures were studied by placing the sintered samples under Scanning electron microscope. Micrographs of the sintered samples are depicted in Fig. 2 (a-c), shows the surface structure for sintered samples of Mg<sup>+2</sup> doped NiFe<sub>2</sub>O<sub>4</sub> ferrite. Optical micrographs show the fine nature of the particles with some agglomerated dense structure. Micrographs show the presence of larger grains with a number of interfaces, which further affects, dielectric and magnetic properties of these ferrites.

### 3.2 Dielectric studies

The real part ( $\epsilon'$ ) of the complex permittivity is known as dielectric constant and the imaginary part ( $\epsilon''$ ) is attributed to the dielectric loss of the material. Main reason for the emergence of dielectric loss is the lag of the response of materials to the external field.

Variation of Real and imaginary part of permittivity ( $\epsilon'$ ), ( $\epsilon''$ ) and ac conductivity ( $\sigma_{ac}$ ) with frequency at room temperature for the Pure  $NiFe_2O_4$  ferrite and  $Mg^{+2}$  doped ferrite is shown in Fig.3. From the Fig.3 (a), it is clear that  $\epsilon'$  decreases with increasing step change at lower frequencies and remains almost independent at higher frequencies. Variation of dielectric constant with applied frequency is due to charge transport relaxation. Observed dielectric dispersion is attributed to Maxwell and Wagner type interfacial polarization [19-21], as the dielectric constant is a combined effect of dipolar, electronic, ionic and interfacial polarizations. Since ionic polarization decreases with frequency, at higher frequency cycle rates, the constituent electric dipoles are unable to follow the quick variations of the alternating applied electric field and hence, measured  $\epsilon'$  also decreased with frequency. Higher magnitudes of  $\epsilon'$  are related with space charge polarization at grain boundary and heterogeneous dielectric structure.

These inhomogenities arise from synthesis techniques, sintering temperature, impurities, grain structure and pores. By electron exchange between  $Fe^{+2}$  and  $Fe^{+3}$ , displacement of electrons takes place with the applied field and these electrons determine polarization. Polarization decreases with increase in frequency and for further increase, the electric exchange between  $Fe^{+2}/Fe^{+3}$  cannot follow the alternating field hence reaches the constant value [22-23].

Gradation in the dielectric loss for all the proposed series of samples upto the frequency range 1 MHz at room temperature is shown in Fig. 3(c). Values of loss tangent ( $\tan\delta$ ) represent the attenuation in magnetoelectrics and polarization being unable to respond to applied external frequency. The nature of curves for both  $\epsilon'$  and  $\tan\delta$  are almost similar and may be correlated to the domain wall motion with the applied field. the electron exchange between  $Fe^{+2}$  and  $Fe^{+3}$  ions can correlate with the dielectric properties exhibited by proposed samples.

In order to understand the type of charge carriers and type of polarons responsible for conduction, ac conductivity,  $\sigma_{ac}$  were estimated as per  $\sigma_{ac} = \omega \epsilon_0 \epsilon''$ , with  $\epsilon_0$  is the permittivity of free space and  $\omega = 2\pi f$ .

Variation of  $\sigma_{ac}$  with frequency,  $f$ , is shown in Fig.3 (a-d) for all the synthesized samples. Obtained plots are linear for almost entire range of frequency except at lower frequencies. Linear variation of  $\sigma_{ac}$  with frequency confirms that, conduction in mixed spinel ferrite occurs by the hopping of charge carriers between the localized states which confirms the small polaron type of conduction [24-25]. Conduction mechanism in spinel ferrites can be explained based on the hopping of charge carriers between  $Fe^{+2}$  and  $Fe^{+3}$  ions on octahedral lattice sites. Increase in the frequency of the applied field accelerates the hopping of charge carriers thereby enhancing the overall conduction process, thereby increasing the conductivity. At higher frequencies,  $\sigma_{ac}$  remains constant because the hopping frequency of the charge carriers no longer follows the external applied field variations and lags behind it. However, the decrease in conductivity values at lower frequencies can be correlated to conduction by mixed polarons.

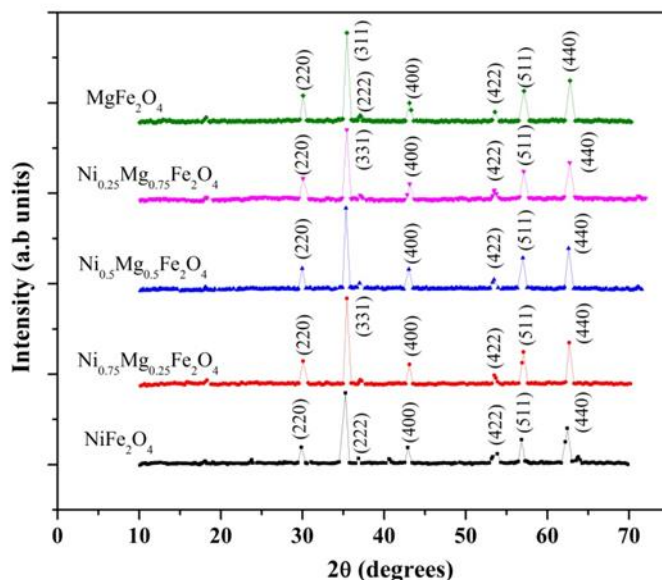


Fig. 1 Diffractogram of  $Mg^{+2}$  doped nano  $NiFe_2O_4$  powder samples

Table 1(a). Structural Parameters of Mg<sup>+2</sup> doped NiFe<sub>2</sub>O<sub>4</sub>, obtained from the X-ray diffractogram.

Samples	X-ray Density ( $\rho_{XRD}$ ) gm/cm <sup>3</sup>	Crystallite size (nm)	Lattice constant 'a' (Å)	Volume of Unit cell (Å <sup>3</sup> )	Hopping Length at A-Site (L <sub>A</sub> ) in (Å)	Hopping Length at B-Site (L <sub>B</sub> ) in (Å)
NiFe <sub>2</sub> O <sub>4</sub>	5.197	27.04	8.433	599	3.651	2.981
Ni <sub>0.75</sub> Mg <sub>0.25</sub> Fe <sub>2</sub> O <sub>4</sub>	5.083	24.82	8.393	590	3.634	2.967
Ni <sub>0.5</sub> Mg <sub>0.5</sub> Fe <sub>2</sub> O <sub>4</sub>	4.856	24.77	8.415	594	3.643	2.974
Ni <sub>0.25</sub> Mg <sub>0.75</sub> Fe <sub>2</sub> O <sub>4</sub>	4.680	23.52	8.393	592	3.634	2.967
MgFe <sub>2</sub> O <sub>4</sub>	4.502	23.9	8.392	590	3.634	2.966

Table 1(b).

Samples	L <sub>A</sub> (Å)	L <sub>B</sub> (Å)	d <sub>AO</sub> (Å)	d <sub>BO</sub> (Å)	d <sub>AE</sub> (Å)	d <sub>BE</sub> (Å)	d <sub>BEU</sub> (Å)
NiFe <sub>2</sub> O <sub>4</sub>	3.6516	2.9811	1.8258	2.1083	5.9670	2.9835	2.9835
Ni <sub>0.75</sub> Mg <sub>0.25</sub> Fe <sub>2</sub> O <sub>4</sub>	3.6344	2.9671	1.8172	2.0967	9.9343	2.9671	2.9671
Ni <sub>0.5</sub> Mg <sub>0.5</sub> Fe <sub>2</sub> O <sub>4</sub>	3.6438	2.9748	1.0519	2.1021	5.9496	2.9748	2.9748
Ni <sub>0.25</sub> Mg <sub>0.75</sub> Fe <sub>2</sub> O <sub>4</sub>	3.6344	2.9671	1.8172	2.0967	9.9343	2.9671	2.9671
MgFe <sub>2</sub> O <sub>4</sub>	3.6340	2.9668	1.8170	2.0965	5.9337	2.9668	2.9668

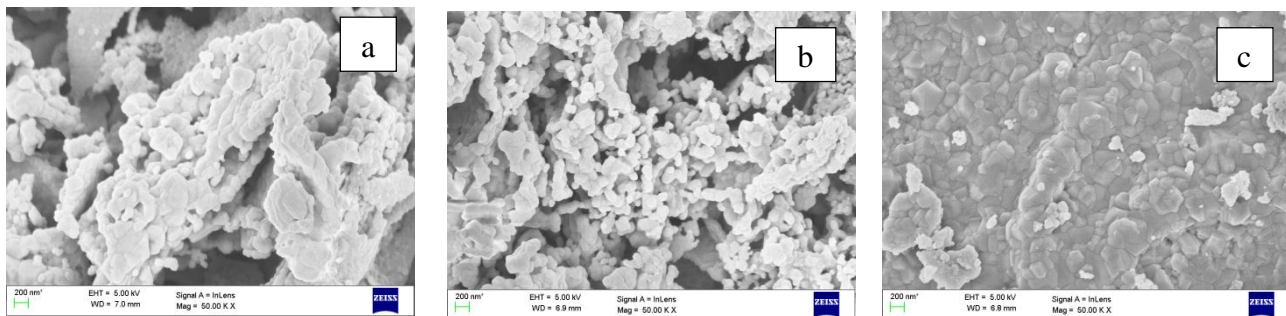


Fig. 2 FESEM Micrographs for (a) Ni<sub>0.75</sub>Mg<sub>0.25</sub>Fe<sub>2</sub>O<sub>4</sub> (b) Ni<sub>0.5</sub>Mg<sub>0.5</sub>Fe<sub>2</sub>O<sub>4</sub> and (c) Ni<sub>0.25</sub>Mg<sub>0.75</sub>Fe<sub>2</sub>O<sub>4</sub>

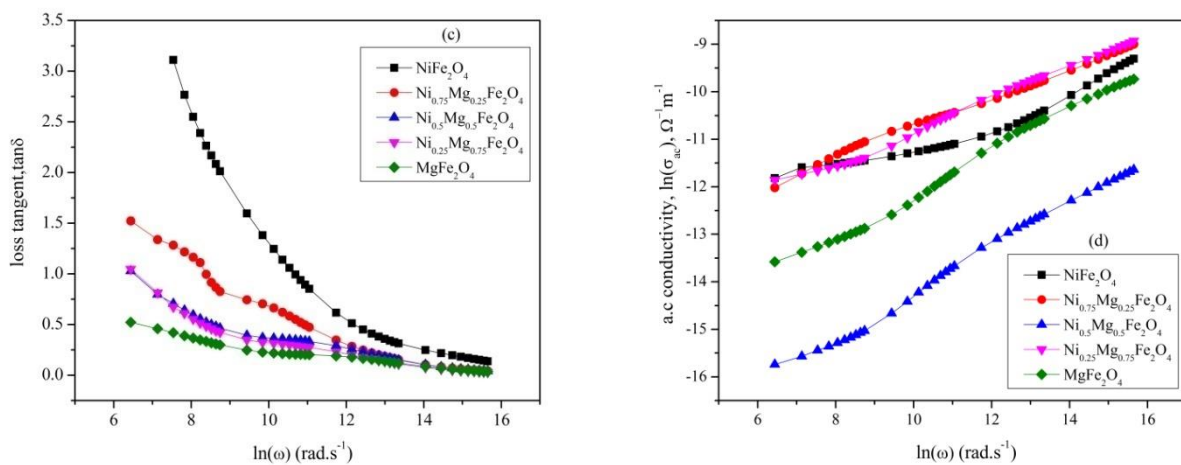


Fig.3

(a).Real Part of permittivity,  $\epsilon'$  with  $\ln(\omega)$ , (b)Imaginary Part of permittivity, $\epsilon''$  with  $\ln(\omega)$ , (c) Tangent loss factor  $\tan\delta$  with  $\ln(\omega)$  and (d) AC conductivity, $\sigma_{ac}$  with  $\ln(\omega)$ .

### 3.3 Magnetic studies

Magnetic hysteresis loops, at room temperature were recorded for all the sintered samples. Magnetic hysteresis loops for all the samples sintered at 900°C are shown in Fig.4. Synthesized and sintered samples exhibited no hysteresis, which may be attributed to super paramagnetic nature of the samples. Various magnetic parameters such as saturation magnetization ( $M_s$ ), remanence magnetization ( $M_r$ ), coercive fields ( $H_c$ ) and squareness ratio ( $SQR=M_r/M_s$ ) were extracted from the obtained M-H loops. Extracted magnetic parameters for all the samples are listed in Table 2. It is observed that, saturation magnetization ( $M_s$ ) decreases with the increase of  $Mg^{+2}$  concentration [26-29]. It is clear that the increasing in the concentration of  $Mg^{+2}$  results a decrease in the saturation magnetization ( $M_s$ ) and remanence magnetization ( $M_r$ ) of  $NiFe_2O_4$ . In case of spinel structured ferrites, the magnetic ordering is by super exchange interactions between the metal ions distributed in the tetrahedral-A site and octahedral-B site. Saturation magnetization decreases as the iron goes to the tetrahedral- A site. This may be based on the fact that the exchange interaction between A and B sites gets weak, resulting in improving of B-B interaction and weakening of A-B interaction, which results in decreasing of saturation magnetization [30-31]

The  $M_r/M_s$  ratio, called the squareness ratio, gives information about the squareness of the hysteresis. Calculated SQR values for all the sintered samples are below 0.5 value, corresponding to the single domain particles with easy axis being randomly oriented [32]. For each sintered sample, experimental values of magnetic moment per formula unit,  $\eta_{exp}$  were calculated as per the relation [33]:  $\eta_{exp} = M_w M_s / 5585$ , here  $M_w$  is the molecular weight of each sample and  $M_s$  is the saturation magnetization.

Magneto crystalline anisotropy constant (K) for the sintered samples can be computed using the saturation magnetization ( $M_s$ ) is given by the relation [34]. Magnetic anisotropy is directly proportional to the coercive force and can be noticed from the obtained magnetic parameters.

$$H_c = 0.96 K / M_s \quad (6)$$

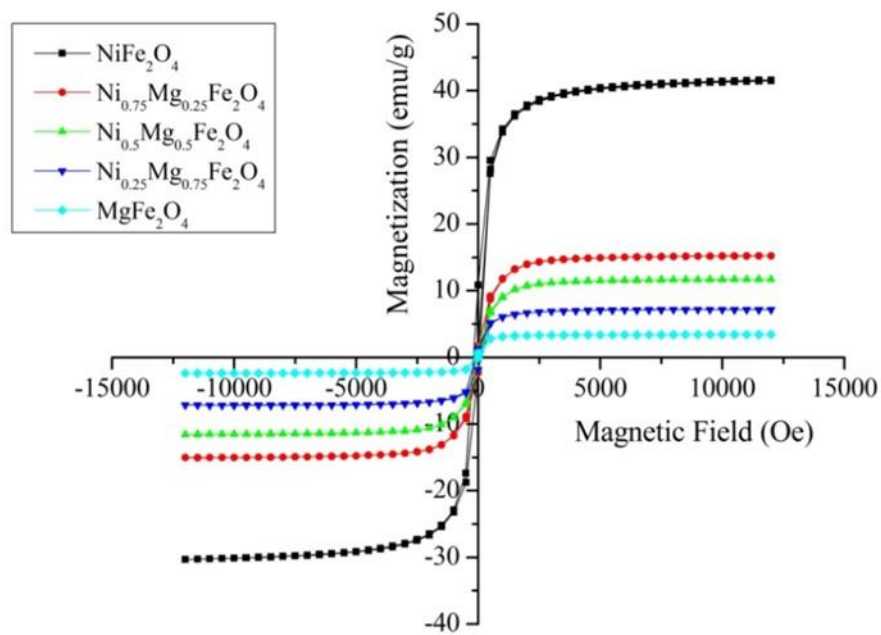


Fig.4. Magnetic Hysteresis loops of  $Mg^{+2}$  doped nano  $NiFe_2O_4$

Table 2. Magnetic parameters extracted from M-H Loops.

Ferrite compositions	Saturation Magnetization ( $M_s$ -emu/g)	Remanance Magnetization ( $M_r$ -emu/g)	Coercive Field ( $H_c$ -Oe)	Squareness Ratio $SQR=M_r/M_s$	Magnetic Moment $\eta_{exp}$ in ( $\mu_B$ )	Anisotropy Constant (K) in erg/gm
NiFe <sub>2</sub> O <sub>4</sub>	34.14	9.12	36.18	0.2681	1.42	1281.75
Ni <sub>0.75</sub> Mg <sub>0.25</sub> Fe <sub>2</sub> O <sub>4</sub>	15.21	1.71	106.98	0.1123	0.61	1695.95
Ni <sub>0.5</sub> Mg <sub>0.5</sub> Fe <sub>2</sub> O <sub>4</sub>	11.79	1.33	103.41	0.1128	0.45	1293.82
Ni <sub>0.25</sub> Mg <sub>0.75</sub> Fe <sub>2</sub> O <sub>4</sub>	7.22	1.24	133.16	0.1745	0.26	6.39
MgFe <sub>2</sub> O <sub>4</sub>	3.36	0.87	15.83	0.375	0.12	55.82

## CONCLUSIONS

Mg<sub>x</sub>Ni<sub>1-x</sub>Fe<sub>2</sub>O<sub>4</sub>(x=0, 0.25, 0.5, 0.75, 1) samples prepared by auto-combustion method exhibited single phase spinel cubic structure. Mean crystallite sizes for the sintered mixed ferrites were calculated using Debye Sherrer formula and are less than 30nm, indicating that the synthesized ferrites are nano in nature. Magnitude of lattice constant for the synthesized samples are in the range of 8.4333Å to 8.3928Å. FESEM results reveals that the morphology of the Mg<sup>+2</sup>doped NiFe<sub>2</sub>O<sub>4</sub> nano-particles are nearly spherical in shape. From the dielectric studies, dielectric dispersion with frequency was observed, and it was explained on the basis of electron-hole hopping mechanism in the light of Maxwell-Wagner two layer models and Koop's theory. Further from tanδ Vs ln(ω) curves, it is observed that the dielectric loss tangent decreases with increase of frequency and all the sintered samples exhibit low values of loss, which is very essential in designing electronic circuits and applications. A.C conductivity ln(σ<sub>ac</sub>) of the proposed samples were plotted against ln(ω), the plots are linear for almost entire range of frequency except at low frequencies. Linear variation of σ<sub>ac</sub> with frequency indicates that the electrical conduction occurs because of the hopping of charge carriers between the localized states which confirms the conduction is due to small polarons. From magnetic studies, it is observed that, the samples with narrow hysteresis loop were synthesized with low values of coercivity. Hence, these ferrites are magnetically soft materials.

These characteristics of the proposed nano-structured ferrites are essential for their use in various electronic device applications such as inductor cores, recording heads and shielding the electromagnetic interference.

## ACKNOWLEDGEMENTS

Authors are highly thankful to STIC, Cochin and CENSE, IISc-Bangalore for providing PXRD and FESEM facilities to accomplish this research work.

## REFERENCES

- 1) M.H.Sousa, E.Hasmonay, J.Depeyrot, F.A.Tourinho, J.C Bacri, E.Dubois, R.Perzynski,
- 2) Y.L Raikherb, J.Magn.Magn.Mater 242, 572-574 (2002).
- 3) C.G Ramankutty, S.sugunan, Appl.Catal.A 218, 39-51 (2001).
- 4) V.Sepelak, K.Baabe, K.Mienert, K.Schultze, F.Krumeich, F.J. Litterst, K.D Becker,
- 5) J.Magn.Magn.Mater 257, 377-386 (2003).
- 6) Maaz K, Duan J.L, Karim S, Chen Y H, Zhai P.E, Xu L.J, Yao H.J, Liu Jour.Alloys. Comp, 684, 656-662 (2016).
- 7) N.Mo, Y.Y.Song, C.E Patton, J.Appl.Phys 97, 93901 (2005).
- 8) Mathubala G, Manikandan A, Arul Antony S, Ramar P, J.Mol.Struct, 113, 79-87 (2016).
- 9) Koseoglu. Y, Ceramic Int, 39, 4221-4230 (2013).
- 10) Marina T.F, Chicinas I, Isnard O, Neamlu B.V, Ceramic Int, 42, 4754-4763 (2016).
- 11) Shobana M.K, Sankar S, Jour.Magn.Magn.Mater, 321, 2125-2128 (2009).
- 12) S Sundar Manoharan and K C Patil, Jourl.Solid State Chem, 102, 267-276 (1993).
- 13) N Arul Dhas and K C Patil, Jourl.Solid State Chem, 102, 440-445 (1993).
- 14) S.Abdul Khader, Asiya Parveez, Arka Chaudhuri, M S Shekhawat, T.Sankarappa, Physica B: Physics of Cond. Matter, 584, 411675 (2020).
- 15) S.Singhal, K. Chandra, Jour. Solid State Chem, 180(1), 296-300 (2007).
- 16) R D Shannon, Acta Crystallographica B, 25, 751-767 (1976).
- 17) C.Rao, Chemical Applications of Infrared Spectroscopy, Academic Press New York, NY, USA (1936).

- 18) O.M Hemeda, M.Barakat, D.M Hemeda, Turkish Jour.Phy, 27, 537 (2003).
- 19) Maxwell JC, Electricity & Magnetism, Vol 1, Oxford Univ Press, Oxford (1929).
- 20) Wagner KW (1913) Ann Phys 40:817.
- 21) Koops CG (1951) Phys Rev 83:121
- 22) A Thakur, P Mathur, M.Singh, J.Phy.Chem Solids, 68, 378-381 (2007).
- 23) A.V Ramana Reddy, G.Ranga Mohan, B.S Boyanov, D.Ravinder, Mater.Lett, 39,153-165 (1999).
- 24) A.M Shaik, S.S Bellad, B.K Chougule, J.Magn.Magn.Mater, 195, 384-390 (1999).
- 25) N.Rezlescu, S.Istrate, E.Rezlescu, E.Luca, J.Phys.Chem. Solids, 35, 43-46 (1974).
- 26) Hankare P.P, Sankpal U.B, Patil R P, Mulla I S, Sasikala R, Tripathi A.K, J.Alloys.Comp, 496, 256-260 (2010).
- 27) Thomas J J, Shinde A.B, Krishna P.S, Kalarikkal N, J.Alloys.Comp, 502, 231-237 (2010).
- 28) Raju K, Yoon D H, J.Supercond.Magn, 27, 1285-1292 (2014).
- 29) Yoon D H, Muksin, Raju K, J.Supercond.Magn, 29, 439-445 (2016).
- 30) A.C.F.M Costa, M.R Morelli, R.H.G.A Kiminami, Ceram.Trans (7), 321-332 (2003).
- 31) Alex Goldman, Modern Ferrite Technology, 2 nd Ed, New York (2006).
- 32) Suresh J, Trinadh B, Babu B.V, Reddy P.V.S.S.N Mohan B.S, Krishna A R, Samatha K, Phy.B. Condens.Matter, 620, 413264 (2021).
- 33) B.Parvatheeswara Rao, P.S.V Subba Rao, K.H Rao, IEEE Transactions on Magnetics, 33(6), 4454-4458 (1997).
- 34) S.Singhal, K.Chandra, J.Solid State Chem 180(1), 296-300 (2007).

Figures

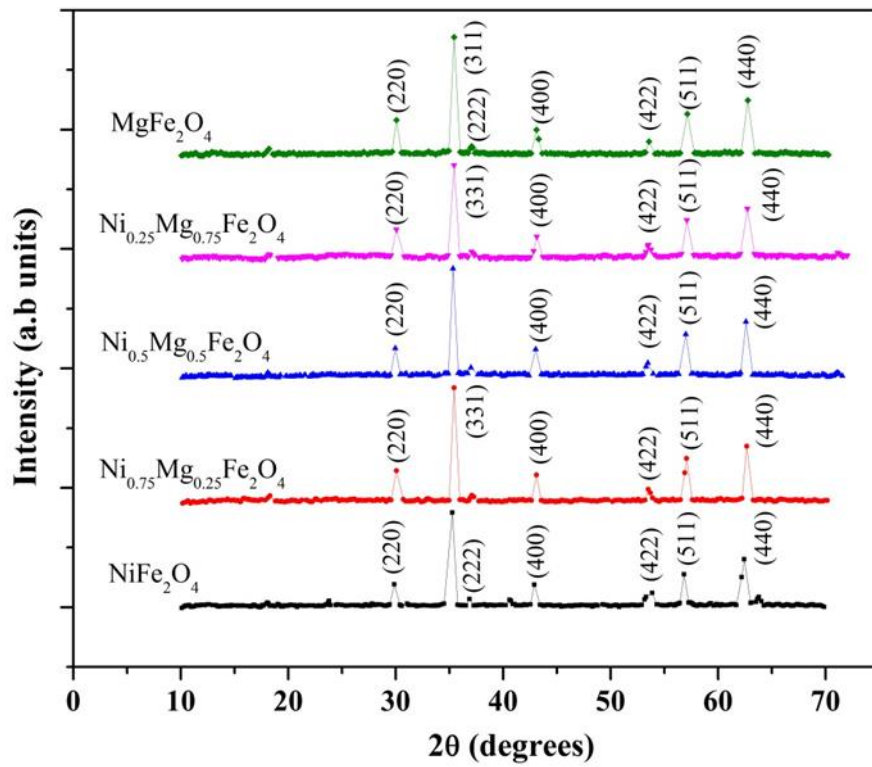


Fig. 1 Diffractogram of Mg<sup>+2</sup> doped nano NiFe<sub>2</sub>O<sub>4</sub> powder samples

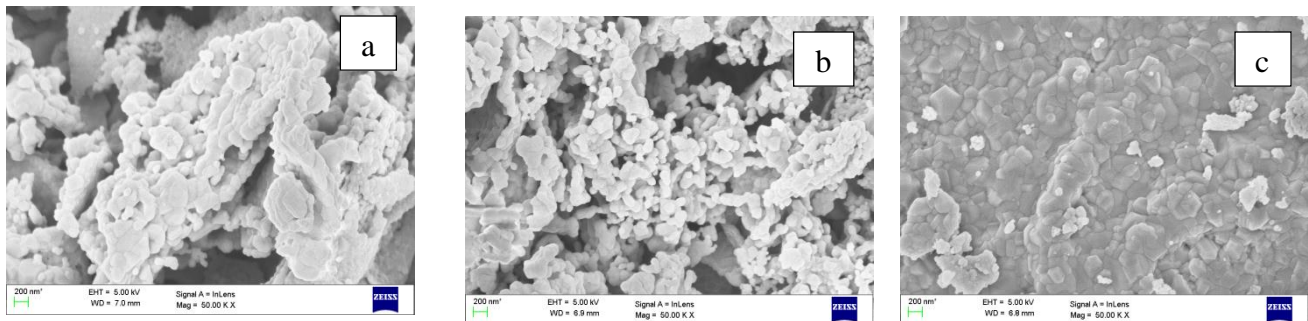


Fig. 2 FESEM Micrographs for (a) Ni<sub>0.75</sub>Mg<sub>0.25</sub>Fe<sub>2</sub>O<sub>4</sub> (b) Ni<sub>0.5</sub>Mg<sub>0.5</sub>Fe<sub>2</sub>O<sub>4</sub> and (c) Ni<sub>0.25</sub>Mg<sub>0.75</sub>Fe<sub>2</sub>O<sub>4</sub>

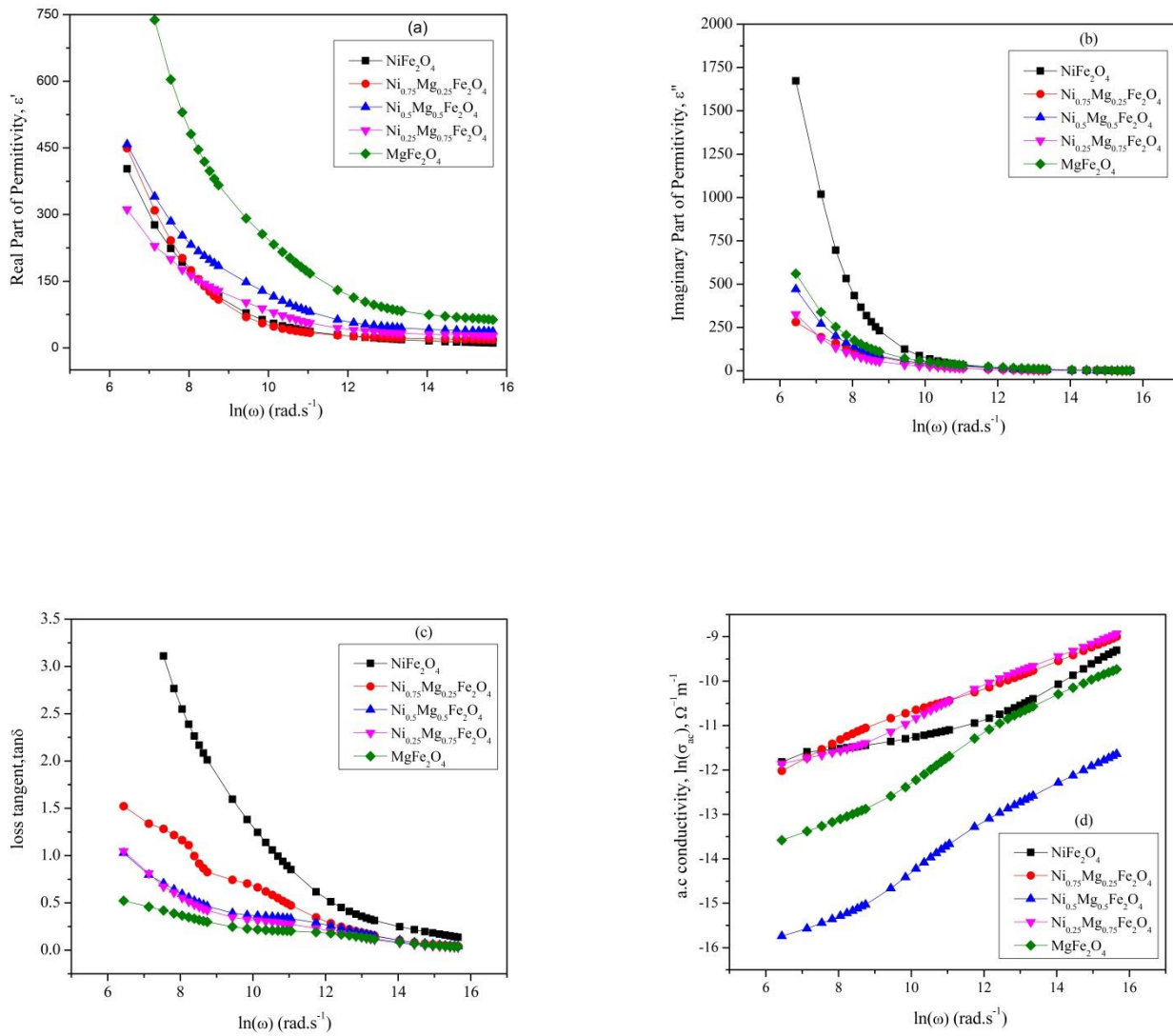


Fig.3 (a).Real Part of permittivity,  $\epsilon'$  with  $\ln(\omega)$  , (b)Imaginary Part of permittivity, $\epsilon''$  with  $\ln(\omega)$  , (c) Tangent loss factor  $\tan\delta$  with  $\ln(\omega)$  and (d) AC conductivity, $\sigma_{ac}$  with  $\ln(\omega)$ .

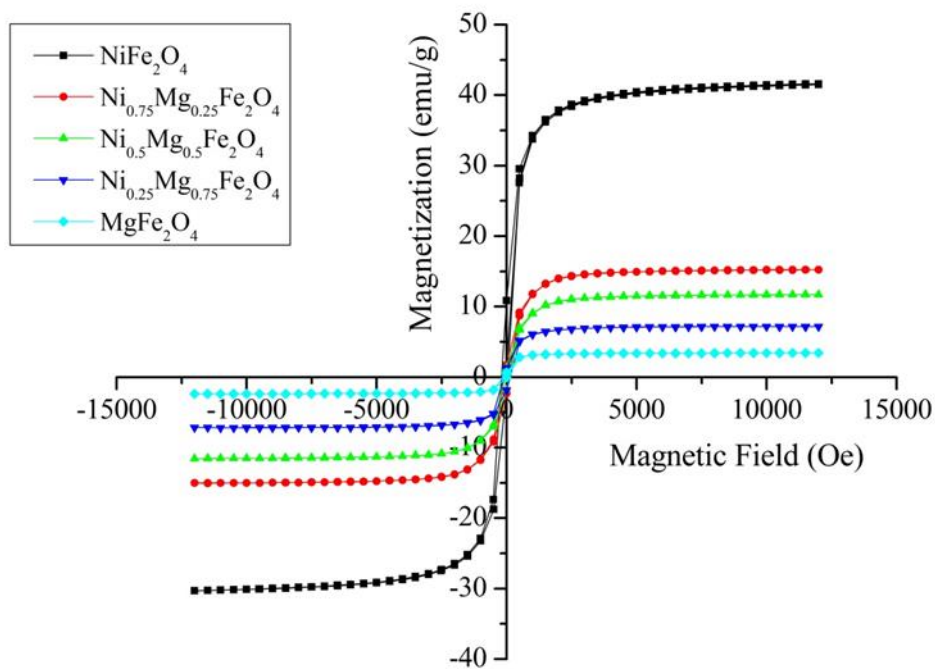


Fig.4. Magnetic Hysteresis loops of  $Mg^{+2}$  doped nano  $NiFe_2O_4$

**Tables**

Table 1(a). Structural Parameters of  $Mg^{+2}$  doped  $NiFe_2O_4$ , obtained from the X-ray diffractogram.

Samples	X-ray Density ( $\rho_{XRD}$ ) gm/cm <sup>3</sup>	Crystallite size (nm)	Lattice constant 'a' ( $\text{\AA}$ )	Volume of Unit cell ( $\text{\AA}^3$ )	Hopping Length at A-Site ( $L_A$ ) in ( $\text{\AA}$ )	Hopping Length at B-Site ( $L_B$ ) in ( $\text{\AA}$ )
$NiFe_2O_4$	5.197	27.04	8.433	599	3.651	2.981
$Ni_{0.75}Mg_{0.25}Fe_2O_4$	5.083	24.82	8.393	590	3.634	2.967
$Ni_{0.5}Mg_{0.5}Fe_2O_4$	4.856	24.77	8.415	594	3.643	2.974
$Ni_{0.25}Mg_{0.75}Fe_2O_4$	4.680	23.52	8.393	592	3.634	2.967
$MgFe_2O_4$	4.502	23.9	8.392	590	3.634	2.966

Table 1(b).

Samples	$L_A$ ( $\text{\AA}$ )	$L_B$ ( $\text{\AA}$ )	$d_{AO}$ ( $\text{\AA}$ )	$d_{BO}$ ( $\text{\AA}$ )	$d_{AE}$ ( $\text{\AA}$ )	$d_{BE}$ ( $\text{\AA}$ )	$d_{BEU}$ ( $\text{\AA}$ )
$NiFe_2O_4$	3.6516	2.9811	1.8258	2.1083	5.9670	2.9835	2.9835
$Ni_{0.75}Mg_{0.25}Fe_2O_4$	3.6344	2.9671	1.8172	2.0967	9.9343	2.9671	2.9671
$Ni_{0.5}Mg_{0.5}Fe_2O_4$	3.6438	2.9748	1.0519	2.1021	5.9496	2.9748	2.9748
$Ni_{0.25}Mg_{0.75}Fe_2O_4$	3.6344	2.9671	1.8172	2.0967	9.9343	2.9671	2.9671
$MgFe_2O_4$	3.6340	2.9668	1.8170	2.0965	5.9337	2.9668	2.9668

Table 2. Magnetic parameters extracted from M-H Loops.

Ferrite compositions	Saturation Magnetization ( $M_s$ -emu/g)	Remanance Magnetization ( $M_r$ -emu/g)	Coercive Field ( $H_C$ -Oe)	Squareness Ratio $SQR=M_r/M_s$	Magnetic Moment $\eta_{exp}$ in ( $\mu_B$ )	Anisotropy Constant (K) in erg/gm
NiFe <sub>2</sub> O <sub>4</sub>	34.14	9.12	36.18	0.2681	1.42	1281.75
Ni <sub>0.75</sub> Mg <sub>0.25</sub> Fe <sub>2</sub> O <sub>4</sub>	15.21	1.71	106.98	0.1123	0.61	1695.95
Ni <sub>0.5</sub> Mg <sub>0.5</sub> Fe <sub>2</sub> O <sub>4</sub>	11.79	1.33	103.41	0.1128	0.45	1293.82
Ni <sub>0.25</sub> Mg <sub>0.75</sub> Fe <sub>2</sub> O <sub>4</sub>	7.22	1.24	133.16	0.1745	0.26	6.39
MgFe <sub>2</sub> O <sub>4</sub>	3.36	0.87	15.83	0.375	0.12	55.82